


Surface morphology and active sites of TiO₂ for photoassisted catalysis

Bhaskar Soman¹ · Swapna Challagulla² · Soumitra Payra² · Srikanta Dinda¹ · Sounak Roy² 

Received: 7 October 2017 / Accepted: 4 December 2017 / Published online: 15 December 2017
© Springer Science+Business Media B.V., part of Springer Nature 2017

Abstract The main aim of this work is to discriminate the closely related adsorption and catalytic degradation processes that occur during a photocatalytic reaction. Very high-surface-area TiO₂ and Pd-doped TiO₂ were synthesized by microwave-assisted hydrothermal synthesis and used for degradation of methylene blue as a model pollutant dye. Thorough structural, morphological, and surface analyses of the synthesized catalysts were conducted to investigate key material properties that influence adsorption and catalytic performance. The adsorption capacity of the catalysts was determined by fitting adsorption data using the Langmuir isotherm model, and the photocatalytic activity of the synthesized samples was evaluated by periodically measuring the concentration of methylene blue as it was photocatalytically degraded under ultraviolet (UV) light. The results indicated that noble-metal incorporation compromised adsorption but favored catalytic performance.

Keywords Microwave synthesis · TiO₂ · Photocatalysis · Methylene blue degradation · Surface porosity · Active site

Introduction

Organic and inorganic substances, particularly in wastewater from textile industries, represent a main source of environmental pollution. Different types of dye have adverse impacts on the environment due to their toxic and carcinogenic nature [1,

✉ Sounak Roy
sounak.roy@hyderabad.bits-pilani.ac.in

¹ Department of Chemical Engineering, Birla Institute of Technology and Science (BITS) Pilani, Hyderabad Campus, Jawahar Nagar, Shameerpet Mandal, Hyderabad 500078, India

² Department of Chemistry, Birla Institute of Technology and Science (BITS) Pilani, Hyderabad Campus, Jawahar Nagar, Shameerpet Mandal, Hyderabad 500078, India

2]. As international environmental standards are becoming more stringent, different methods have been developed, including use of coagulants, ultrafiltration, and adsorption techniques, to control or eliminate dyes [3–7]. All the aforementioned methods rely primarily on adsorption of dyes on the surface of a material. In such processes, the adsorbent material will lose its ability as the surface becomes blocked by adsorption, in turn making these techniques unsustainable in the long term. On the other hand, light-assisted degradation of organic pollutants is a promising strategy for environmental remediation. Advanced oxidation processes are innovative and effective approaches for removal and degradation of dyes. Photoassisted catalytic decomposition of organic dye pollutants is an advanced oxidation process in which pollutants are degraded at active sites on the surface of a semiconductor photocatalyst, thus regenerating the surface and making the material both reusable and sustainable [8]. Among the wide range of photocatalysts, TiO_2 is considered to be a leading candidate, as it is nontoxic, thermally stable, relatively cheap, and highly active.

Exhaustive work has been carried out on synthesis of TiO_2 nanoparticles via various routes such as solution combustion [9–11], sol–gel [12, 13], hydrothermal [14], and microwave methods [15], to produce materials with different microstructure and crystallinity, characteristics that significantly control the adsorption capacity and photocatalytic activity of such materials. Researchers have also doped noble metals such as palladium [16], gold [17], silver [18], and platinum [19] as well as anionic dopants such as sulfur [20] and nitrogen [21] for catalytic abatement of dyes. Ismail et al. investigated the effect of mesoporous order and crystallinity of sol–gel-synthesized Pd/TiO_2 on its photocatalytic activity [22]. The enhanced photocatalytic activity of combustion-synthesized TiO_2 catalyst was attributed to its crystallinity, nanosize, and surface area by Nagaveni et al. [23]. Sangpour et al. [18] studied the enhanced dye degradation on noble metal (Cu/Ag/Au)-doped TiO_2 compared with undoped TiO_2 thin films. Similar observations were also reported by others [17, 24–29]. Detailed studies on ultrafast, high adsorption of dyes or other pollutants on $\text{Fe}_3\text{O}_4/\text{SiO}_2$ or reduced graphene oxide or WO_3/C nanowires have also been carried out, mostly revealing that adsorption takes place in agreement with the pseudo-second-order Langmuir or Freundlich isotherms [30–32]. Moreover, detailed mechanistic studies have been carried out on degradation of dye over $\text{Fe}_3\text{O}_4/\text{MnO}_2$ [33] or graphene@ TiO_2 catalysts [34]. However, other than a few exceptions [35], existing literature largely does not address differences between surface adsorption and gradual poisoning over time or the catalytic activity of materials for efficient degradation of dyes and regeneration of the surface. There is a need for such studies, as in the long term, poisoned/deactivated material must be replaced, which is not an economically and logistically viable process. Salibye et al. studied adsorption and degradation of methylene blue on hydrogen titanate nanofibers as well as the recyclability and recoverability of the nanofibers [35]. Du and Zheng reported maximum adsorption capacity of 54.29 mg g^{-1} and degradation of about 82% for methylene blue on TiO_2 -halloysite adsorbents after 4 h of irradiation [36].

In this work, we studied the performance of noble metal (Pd)-doped and undoped TiO_2 catalysts for photocatalytic degradation of methylene blue as a representative

dye, and also elucidated the differences in the abatement of adsorption and degradation.

Experimental

Various parameters of TiO₂ can be tuned using different synthesis methods as a fundamental tool, with the microwave-assisted hydrothermal method representing a rapid one-pot synthesis technology. Microwave dielectric heating enhances not only the rate of formation but also the yield of highly pure, high-surface-area nanomaterials. In this work, Pd-doped and pristine TiO₂ were synthesized using a customized microwave-assisted hydrothermal method. Titanium(IV) isopropoxide (TIPO) and palladium nitrate were procured from Sigma Aldrich and used as received. Palladium acetate was purchased from Alfa Aesar, and oxalic acid, urea, and potassium dichromate were purchased from SD Fine Chemicals and used as received without further purification. For synthesis of pristine TiO₂ by microwave method, 0.592 mL TIPO and 0.6 g urea (in 1:5 molar ratio of Ti to urea) in aqueous solution was placed in a sealed microwave vial in a microwave reactor (Monowave 300 GmbH, Europe). The reactor was operated at 850 W, and the reaction mixtures were subjected to temperature of 130 °C for 2 h with stirring at 850 rpm. After microwave treatment, the obtained solid product was filtered off, washed with distilled water and ethanol, and dried to obtain pristine TiO₂. A similar procedure was followed for microwave-assisted synthesis of 5% Pd/TiO₂ (MW) by adding 17.3 mg palladium(II) nitrate to the precursor solution. An impregnation method was also used for synthesis of 5% Pd/TiO₂. Physically impregnated 5% Pd/TiO₂ (IMP) was synthesized by mixing 100 mg microwave-synthesized TiO₂ with 10.5 mg palladium(II) acetate and grinding using a mortar and pestle. The ground powders were calcined at 250 °C for 2 h. The calcination temperature was confirmed by thermogravimetric analysis (TGA) of palladium(II) acetate in aerobic atmosphere (Fig. 1), revealing that the organic part combusted by 250 °C to yield PdO.

TGA measurements were performed using a Shimadzu DTG-60 at scan rate of 10 °C/min in air atmosphere. Rigaku Ultima IV X-ray diffractometer (XRD) with Cu K_α radiation ($\lambda = 1.5418 \text{ \AA}$) was used to determine the crystal phase and crystallite size of the synthesized TiO₂ catalysts. A typical scan was performed at scan rate of 1°/min with step size of 0.02°. The crystallite size (D) was calculated using Scherrer's formula: $D = \frac{0.9\lambda}{B\cos\theta}$, where B is the full-width at half-maximum, λ is the wavelength of the radiation, and θ is the corresponding angle. FullProf Suite was used for Rietveld refinement of the XRD patterns of the microwave-synthesized catalyst by considering the atomic positions of Pd²⁺ and Ti⁴⁺ as 0.00, 0.25, and 0.375. UniRAM 3300 Raman microscope with incident laser wavelength of 532 nm was used to obtain the Raman spectra of the synthesized materials. The concentration of Pd in the synthesized catalysts was monitored by energy-dispersive X-ray fluorescence (ED-XRF, Epsilon 1; PANalytical). The surface area of the synthesized catalysts was determined using Brunauer–Emmett–Teller (BET) apparatus (MicrotracBEL Corp.) by nitrogen

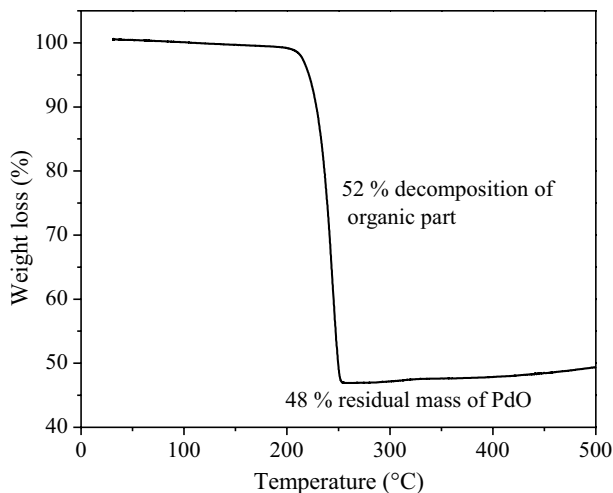


Fig. 1 TGA of palladium(II) acetate in aerobic atmosphere

adsorption/desorption method. JASCO FP-6300 spectrofluorometer was used to study the photoluminescence (PL) of the catalysts at excitation wavelength of 285 nm.

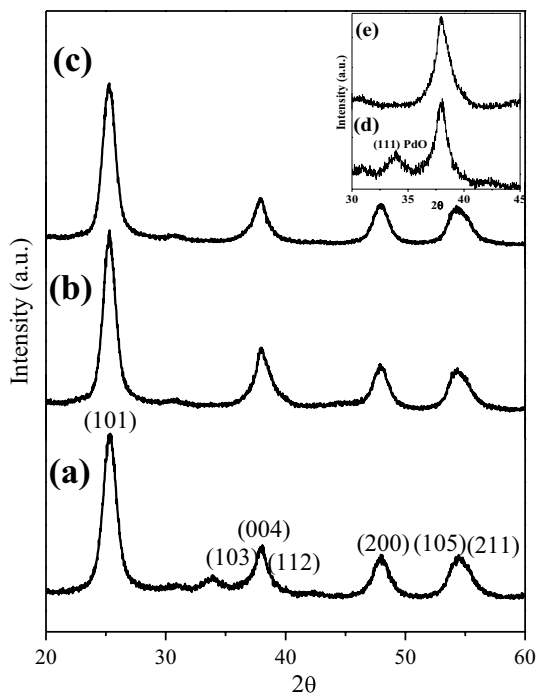
Batch adsorption studies of methylene blue (MB) were carried out using TiO_2 and 5% Pd/ TiO_2 (MW) in a dark enclosure to limit any possibility of photodegradation of the dye. For each adsorption study, the catalyst content was kept constant at 10 mg, and 30 mL aqueous methylene blue solution with concentrations of 5, 10, 20, and 30 ppm was used. The initial and final concentrations of MB were estimated by ultraviolet–visible (UV–Vis) spectroscopy. The amount of MB adsorbed (mg g^{-1}) at equilibrium (q_e) was calculated as $q_e = (C_0 - C_e)V/W$, where C_0 and C_e are the initial and final (equilibrium) concentrations (mg L^{-1}) of methylene blue, and 0.03 L is the volume (V) and 0.01 g is the weight of catalyst (W) used in the adsorption studies.

Photocatalytic degradation studies of methylene blue over the synthesized catalysts were carried out in a cylindrical annular batch reactor housing a 125-W mercury vapor lamp. Water was circulated around the lamp to maintain the reactor at room temperature. MB solution (100 mL, 10 ppm) was placed in the reactor with 25 mg catalyst. As MB is a cationic dye, the pH of the reaction mixture was adjusted to 8.5 for better adsorption. The solution was stirred for 20 min in the dark to allow for adsorption–desorption equilibrium followed by UV irradiation. Aliquots of 3 mL were periodically drawn for analysis. A JASCO V-650 UV–Vis spectrophotometer was used to measure the MB concentration as a function of time to monitor the progress of its photocatalytic degradation. The concentration of the dye was deduced from the maximum adsorption wavelength of MB at 665 nm.

Results and discussion

XRD patterns of the synthesized catalysts are shown in Fig. 2. The undoped and doped TiO₂ were found to crystallize in pure anatase phase [Joint Committee on Powder Diffraction Standards (JCPDS) no. 89-4921] in space group $I4_1/amd$. No peaks corresponding to Pd metal (111) or PdO metal oxide (101) were found in the XRD patterns of the doped sample. For detailed observation of peaks corresponding to Pd or PdO, the inset of Fig. 2 shows the expanded spectrum in the 2θ range from 30° to 45° for 5% Pd/TiO₂ made by microwave method in comparison with its analog synthesized by physical impregnation method. Interestingly, for the impregnated sample, a diffraction peak was observed at 33.9°, corresponding to (101) plane of PdO. This may indicate solid-solution formation by lattice substitution of Pd in TiO₂ matrix in the microwave-synthesized material, or could be due to very high dispersion of the noble metal over the support surface. To probe this further, Rietveld refinements were carried out on the powder diffraction patterns observed for the microwave-synthesized catalysts (Fig. 3). The refined lattice parameters, cell volume, and corresponding χ^2 values obtained from this refinement are presented in Table 1. The ionic radius of Ti⁴⁺ and Pd²⁺ is 68 and 80 pm, respectively [37]; therefore, substitution of Pd²⁺ for Ti⁴⁺ would increase the TiO₂ unit cell volume. However, the refined lattice parameters did not indicate significantly different cell volume, therefore not confirming the lattice substitution. The noble metal could be highly dispersed over the TiO₂ surface. The crystallite size was calculated by

Fig. 2 XRD patterns of **a** 5% Pd/TiO₂ (IMP), **b** 5% Pd/TiO₂ (MW), and **c** pristine TiO₂. Inset shows spectra in 2θ range from 30° to 45° for **d** 5% Pd/TiO₂ (IMP) and **e** 5% Pd/TiO₂ (MW)



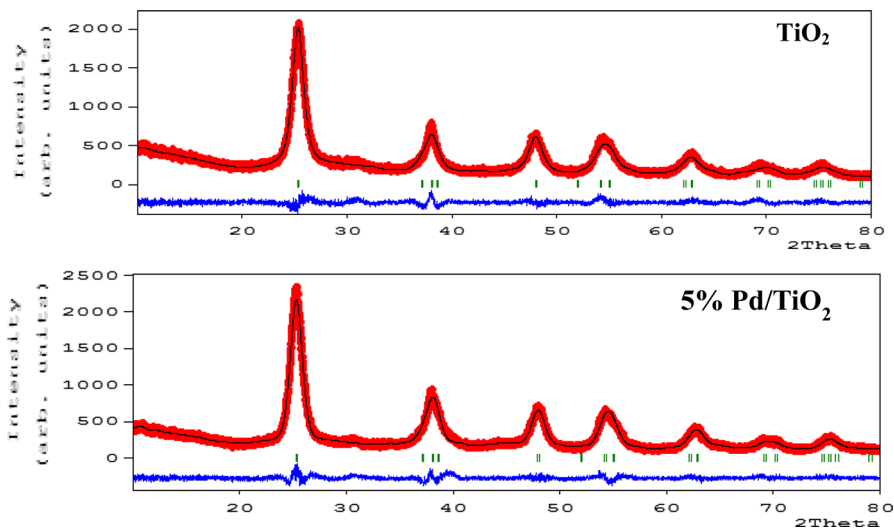


Fig. 3 Rietveld refinement results for powder diffraction patterns of microwave-synthesized catalysts

Table 1 Refined lattice parameters, cell volume, and corresponding χ^2 values obtained from Rietveld refinement

Sample	Cell parameters (Å)			Cell vol. (Å ³)	χ^2	Crystal size (nm)
	<i>a</i>	<i>b</i>	<i>c</i>			
TiO ₂	3.791539	3.791539	9.454658	135.95	1.66	6.49
5% Pd/TiO ₂	3.792864	3.792864	9.446286	135.9	1.76	6.53

using the Debye–Scherrer formula and found to be ~6.5 nm for all the synthesized materials.

Further structural information was extracted from the Raman spectra of the microwave-synthesized materials (Fig. 4). The characteristic peaks at 134, 382, 493, and 614 cm⁻¹ are attributed to the Raman-active vibrational modes of anatase phase with symmetries of E_g , B_{1g} , A_{1g} , and E_g , respectively [38, 39]. No Pd or PdO band was observed for 5% Pd/TiO₂ (MW), indicating high dispersion of the palladium on the TiO₂ matrix, in agreement with the XRD results. Similarly, 5% Pd/TiO₂ (IMP) also did not show any PdO peaks. We performed XRF analysis (Fig. 5) to quantify the Pd concentration in the synthesized catalysts, revealing a value of ~3%.

As catalysis is primarily a surface phenomenon, further investigations were carried out to probe the nature of the surface of the pristine and doped catalysts. Figure 6a shows the N₂ adsorption–desorption isotherms of the pristine TiO₂ and Pd-doped TiO₂. All the isotherms followed the type IV curve of the hysteresis loop, indicating mesoporous nature of the materials. The specific surface area of the doped and undoped TiO₂ was evaluated using BET multipoint analysis; the surface

Fig. 4 Raman spectra of microwave-synthesized and impregnated catalysts

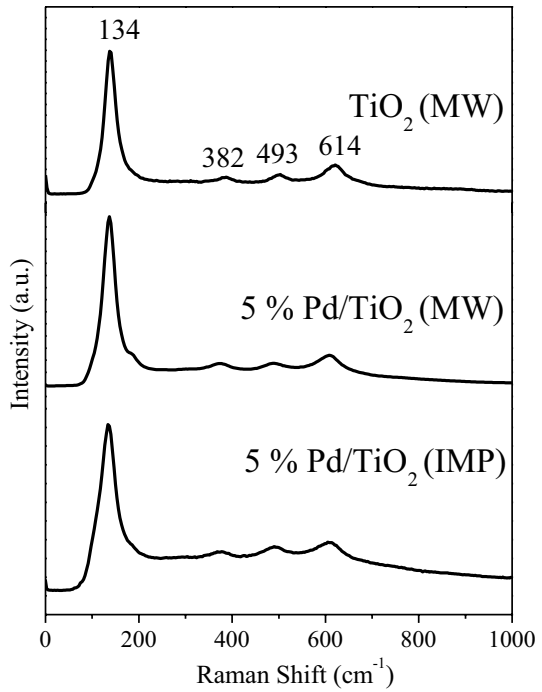
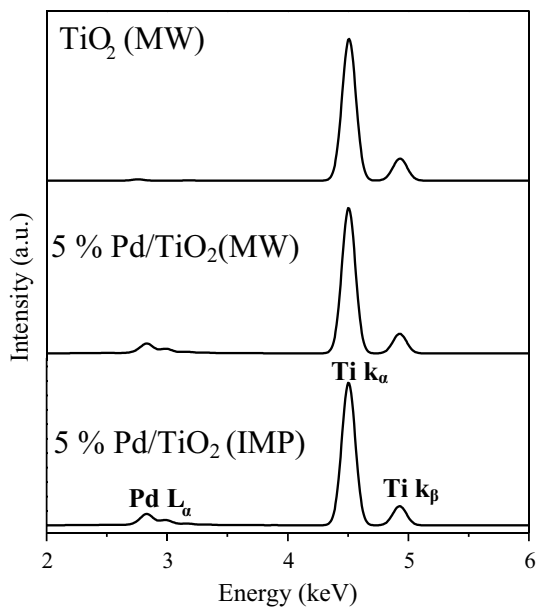


Fig. 5 XRF of microwave-synthesized and impregnated catalysts



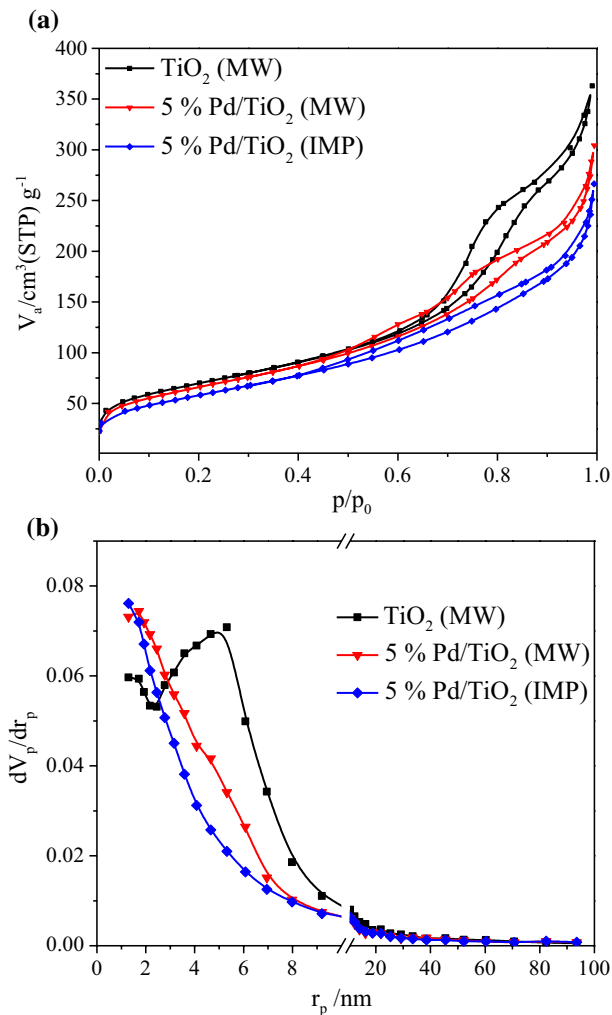


Fig. 6 **a** N_2 adsorption–desorption isotherm, and **b** pore size distribution of microwave-synthesized and impregnated catalysts

Table 2 Surface area, total pore volume, and mean pore size of microwave-synthesized and impregnated catalysts

S. no.	Sample	Surface area ($m^2 g^{-1}$)	Total pore volume ($cm^3 g^{-1}$)	Mean pore size (nm)
1	TiO_2 (MW)	250.7	0.5577	8.8991
2	5% Pd/ TiO_2 (MW)	238.22	0.4433	7.4435
3	5% Pd/ TiO_2 (IMP)	212.99	0.3846	7.2228

area, total pore volume, and mean pore size (Fig. 6b) of all the samples are summarized in Table 2. The BET surface area of 5% Pd/TiO₂ (IMP) was lower than that of 5% Pd/TiO₂ (MW), which in turn was lower than that of pristine TiO₂. One can therefore infer that Pd incorporation reduced the surface area. Moreover, the synthesis method used to obtain the doped samples was also instrumental in determining the surface area. The total pore volume and mean pore size of the doped catalysts were also found to be smaller than those of pristine TiO₂. This may be due to occupancy of the pores in TiO₂ by noble metal, consequently reducing its surface area and porosity. Diffraction studies indicated that Pd in 5% Pd/TiO₂ (MW) was more dispersed than in 5% Pd/TiO₂ (IMP), and this degree of dispersion affected the surface area and porosity of the TiO₂.

Because the photocatalytic properties are determined by electronic properties, the PL emission spectra of the synthesized catalysts were measured and are plotted in Fig. 7a. In PL spectra, higher photoluminescence intensity usually signifies higher electron–hole recombination. Pristine TiO₂ showed higher photoluminescence intensity than the palladium-doped catalysts, indicating that the Pd metal dopant decreased nonradiative recombination of electron–hole pairs, thereby making electrons and holes available for photocatalytic reactions. In semiconducting TiO₂, the valence band (VB) is mostly formed from the O 2*p* orbital, whereas the Ti 3*d* orbital forms the conduction band (CB). The Pd 4*d* orbital level lies below the conduction band of TiO₂. Photoexcited electrons in the CB recombine at a slower rate with holes from the VB due to presence of Pd 4*d* compared with pristine TiO₂, as evidenced by the photoluminescence results. CB electrons may drain to Pd 4*d* due to heterojunctions between TiO₂ and Pd [40]. This may increase the lifetime of photoexcited electrons and holes for effective degradation of methylene blue (Fig. 7b).

Photocatalytic degradation of methylene blue over the synthesized catalysts was performed, and the results are plotted in Fig. 8. For the initial 15 min, the samples were stirred in the dark to attain adsorption-desorption equilibrium, followed by

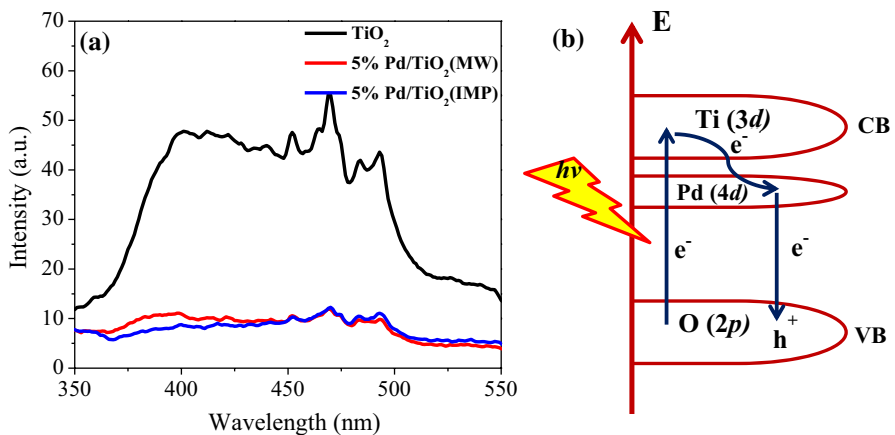


Fig. 7 **a** PL spectra of microwave-synthesized and impregnated catalysts, and **b** schematic illustration of slower electron–hole recombination over 5% Pd/TiO₂ (MW)

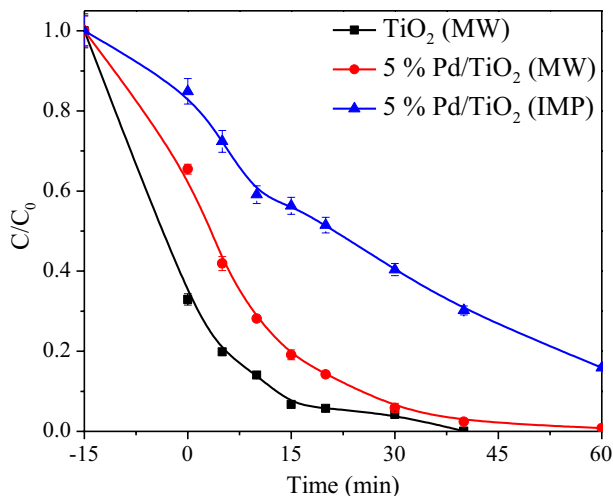


Fig. 8 Photocatalytic degradation of MB over microwave-synthesized catalysts

illumination of light. It is evident from this figure that 5% Pd/TiO₂ (MW) showed poorer performance compared with pristine TiO₂. It can be observed that, in the dark phase, dye adsorption was higher for pristine TiO₂ compared with 5% Pd/TiO₂ (MW). However, with the progress of time under illumination of light, complete degradation of dye over 5% Pd/TiO₂ took exactly the similar time as when using the other, doped and undoped catalysts. It can be concluded from this figure that dye adsorption was higher over undoped TiO₂. This is in accordance with the mesoporous nature of the catalysts. It must be noted that the surface area, pore volume, and size were lower for 5% Pd/TiO₂ (MW) than for pristine TiO₂. Due to the lower pore volume and size, dye adsorption was also lower over 5% Pd/TiO₂ (MW) compared with undoped catalyst. However, the catalytic performance was not affected. Note that the PL spectra indicated lesser electron–hole nonradiative recombination in 5% Pd/TiO₂ (MW) compared with pristine TiO₂, which would help improve the catalysis over 5% Pd/TiO₂ (MW) in spite of its poor adsorption. The 5% Pd/TiO₂ (MW) sample apparently outperformed the impregnated material. This could be due to higher dispersion of Pd metal over the support. The 5% Pd/TiO₂ (IMP) sample with poor dispersion showed great loss of adsorption sites, which was not compensated by its catalytic efficiency. The kinetic data were derived from the degradation profiles under illumination. Figure 9 shows that the degradation of methylene blue over the synthesized catalysts was best fit using the second-order rate equation. The corresponding rate constants obtained for TiO₂ (MW), 5% Pd/TiO₂ (MW), and 5% Pd/TiO₂ (IMP) were 1.04×10^{-3} , 8.98×10^{-4} , and $9 \times 10^{-5} \text{ L mol}^{-1} \text{ s}^{-1}$, respectively.

To confirm the better adsorption of the dye over undoped TiO₂ compared with 5% Pd/TiO₂ (MW) in the dark, the adsorption capacity was measured experimentally over both catalysts. These experimental data were obtained by measuring the amount of methylene blue at equilibrium and the concentration left in solution

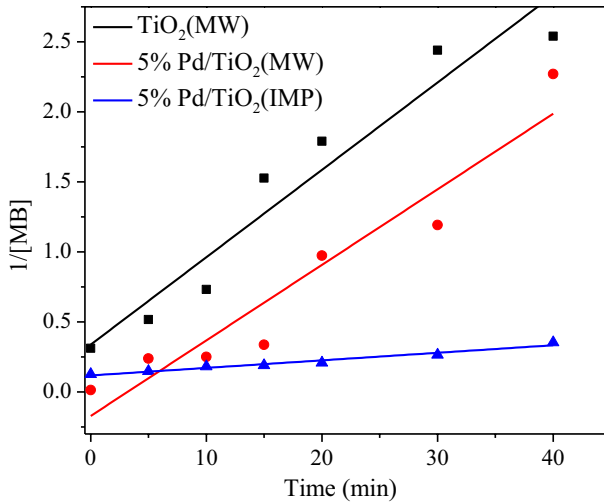


Fig. 9 Kinetics of methylene blue degradation over microwave-synthesized and impregnated catalysts

after adsorption onto the catalyst surface, fitting the results using the Langmuir isotherm model $\frac{C_e}{q_e} = \frac{1}{q_0 b} + \frac{C_e}{q_0}$ (Fig. 10). The plot of C_e/q_e versus C_e yielded meth-

ylene blue adsorption capacity (q_0) values of 66.35 and 27.02 mg g⁻¹ for TiO₂ and 5% Pd/TiO₂ (MW), respectively. It is evident that Pd doping had a negative effect on the adsorption capacity.

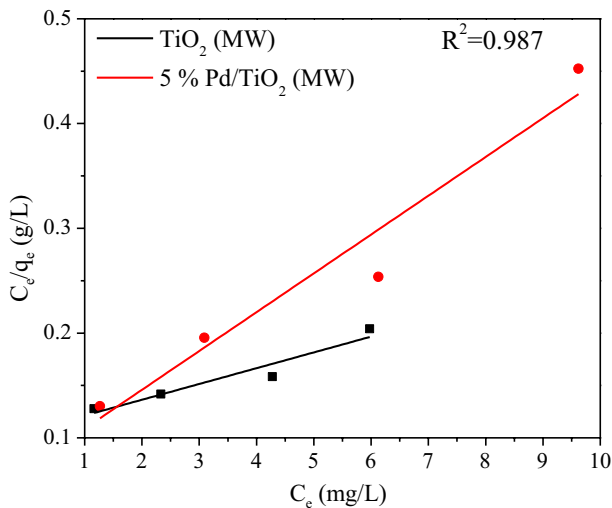


Fig. 10 Langmuir adsorption isotherm model of MB over TiO₂ and 5% Pd/TiO₂ microwave-synthesized catalysts

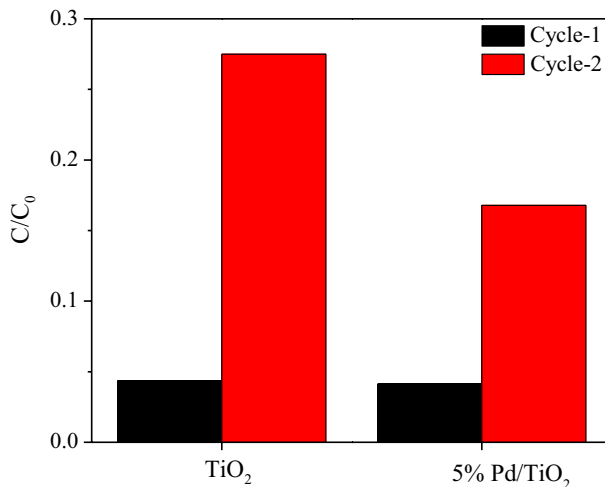


Fig. 11 Recyclability of MB photodegradation over TiO₂ and 5% Pd/TiO₂ catalysts

The improved adsorption capacity of the pristine and Pd-doped TiO₂ samples could lead to blocking of active sites, thereby shortening the life of such catalysts. To investigate this possibility, the recyclability performance of the pristine and 5% Pd/TiO₂ (MW) samples was compared. Figure 11 shows the recyclability of methylene blue photodegradation for two cycles over both catalysts, revealing significantly greater deactivation of TiO₂ in the second cycle compared with Pd/TiO₂. Therefore, it can be concluded that, although the adsorption capacity was affected by the higher Pd loading, the catalytic performance was not compromised.

Conclusions

Pd-doped TiO₂ catalysts were synthesized using microwave and impregnation methods. XRD and Raman spectra showed peaks typical for TiO₂. Rietveld refinement for the microwave-synthesized samples revealed Pd highly dispersed over TiO₂ nanocrystals. BET surface analysis showed that Pd incorporation blocked the pores of mesoporous pristine TiO₂, thereby reducing its surface area. PL spectroscopy of the studied catalysts revealed that Pd doping significantly reduced electron–hole recombination. Therefore, incorporation of Pd affected adsorption negatively but photocatalysis positively, as confirmed by photocatalytic degradation experiments. Recyclability and adsorption studies were carried out, indicating that, even though Pd incorporation negatively affected the adsorption capacity, it improved the catalytic efficacy of the photocatalyst.

Acknowledgements S.R. thanks the Department of Science and Technology (SERB/F/825/2014-15) and CSIR [01(2867/17/EMR-II)] for financial aid. The authors also thank the Department of Science and Technology—fund for improvement of science and technology infrastructure (DST FIST; SR/FST/CSI-240/2012) for procurement of FT-IR and UV–Vis spectroscopy.

References

1. S.S. Auerbach, D.W. Bristol, J.C. Peckham, G.S. Travlos, C.D. Hébert, R.S. Chhabra, *Food Chem. Toxicol.* **48**, 169 (2010)
2. M. Rao, R. Scelza, R. Scotti, L. Gianfreda, J. *Soil Sci. Plant Nutr.* **10**, 333 (2010)
3. N. Kannan, M.M. Sundaram, *Dyes Pigm.* **51**, 25 (2001)
4. V. Gomez, M. Larrechi, M. Callao, *Chemosphere* **69**, 1151 (2007)
5. L. Wang, J. Zhang, A. Wang, *Desalination* **266**, 33 (2011)
6. N. Zaghbani, A. Hafiane, M. Dhabbi, *Sep. Purif. Technol.* **55**, 117 (2007)
7. S. Zhang, H. Gao, J. Li, Y. Huang, A. Alsaedi, T. Hayat, X. Xu, X. Wang, *J. Hazard. Mater.* **321**, 92 (2017)
8. S. Zhang, H. Gao, X. Liu, Y. Huang, X. Xu, N.S. Alharbi, T. Hayat, J. Li, *ACS Appl. Mater. Interfaces* **8**, 35138 (2016)
9. K. Nagaveni, M. Hegde, G. Madras, *J. Phys. Chem. B* **108**, 20204 (2004)
10. S. Roy, A. Marimuthu, M. Hegde, G. Madras, *Appl. Catal. B* **73**, 300 (2007)
11. S. Challagulla, S. Roy, *J. Mater. Res.* **32**, 2764 (2017)
12. R. Nagarjuna, S. Roy, R. Ganesan, *Microporous Mesoporous Mater.* **211**, 1 (2015)
13. S. Challagulla, R. Nagarjuna, R. Ganesan, S. Roy, *J. Porous Mater.* **22**, 1105 (2015)
14. M. Wu, G. Lin, D. Chen, G. Wang, D. He, S. Feng, R. Xu, *Chem. Mater.* **14**, 1974 (2002)
15. A.V. Murugan, V. Samuel, V. Ravi, *Mater. Lett.* **60**, 479 (2006)
16. A.A.A. El-Rady, M.S.A. El-Sadek, M.M.E.-S. Breky, F.H. Assaf, *Adv. Nanopart.* **2**, 372 (2013)
17. C. Quinones, J. Ayala, W. Vallejo, *Appl. Surf. Sci.* **257**, 367 (2010)
18. P. Sangpour, F. Hashemi, A.Z. Moshfegh, *J. Phys. Chem. C* **114**, 13955 (2010)
19. S. Sakthivel, M. Shankar, M. Palanichamy, B. Arabindoo, D. Bahnemann, V. Murugesan, *Water Res.* **38**, 3001 (2004)
20. T. Umebayashi, T. Yamaki, S. Tanaka, K. Asai, *Chem. Lett.* **32**, 330 (2003)
21. N.C. Khang, N. Van Minh, I.-S. Yang, *J. Nanosci. Nanotechnol.* **11**, 6494 (2011)
22. A.A. Ismail, D.W. Bahnemann, L. Robben, V. Yarovy, M. Wark, *Chem. Mater.* **22**, 108 (2009)
23. K. Nagaveni, G. Sivalingam, M. Hegde, G. Madras, *Appl. Catal. B* **48**, 83 (2004)
24. Z. Li, Z. Sun, Z. Duan, R. Li, Y. Yang, J. Wang, X. Lv, W. Qi, H. Wang, *Sci. Rep.* **7**, 42932 (2017)
25. J. Schneider, M. Matsuoka, M. Takeuchi, J. Zhang, Y. Horiuchi, M. Anpo, D.W. Bahnemann, *Chem. Rev.* **114**, 9919 (2014)
26. W. Yao, B. Zhang, C. Huang, C. Ma, X. Song, Q. Xu, *J. Mater. Chem.* **22**, 4050 (2012)
27. C. Hu, Y. Lan, J. Qu, X. Hu, A. Wang, *J. Phys. Chem. B* **110**, 4066 (2006)
28. F. Han, V.S.R. Kambala, M. Srinivasan, D. Rajarathnam, R. Naidu, *Appl. Catal. A* **359**, 25 (2009)
29. S. Naraginti, F.B. Stephen, A. Radhakrishnan, A. Sivakumar, *Spectrochim. Acta Part A* **135**, 814 (2015)
30. P. Wang, X. Wang, S. Yu, Y. Zou, J. Wang, Z. Chen, N.S. Alharbi, A. Alsaedi, T. Hayat, Y. Chen, *Chem. Eng. J.* **306**, 280 (2016)
31. S. Yu, X. Wang, W. Yao, J. Wang, Y. Ji, Y. Ai, A. Alsaedi, T. Hayat, X. Wang, *Environ. Sci. Technol.* **51**, 3278 (2017)
32. S. Zhang, H. Yang, H. Huang, H. Gao, X. Wang, R. Cao, J. Li, X. Xu, X. Wang, *J. Mater. Chem. A* **5**, 15913 (2017)
33. S. Zhang, Q. Fan, H. Gao, Y. Huang, X. Liu, J. Li, X. Xu, X. Wang, *J. Mater. Chem. A* **4**, 1414 (2016)
34. D. Zhao, G. Sheng, C. Chen, X. Wang, *Appl. Catal. B Environ.* **111**, 303 (2012)
35. I. El Saliby, L. Erdei, J.-H. Kim, H.K. Shon, *Water Res.* **47**, 4115 (2013)
36. Y. Du, P. Zheng, *Korean J. Chem. Eng.* **31**, 2051 (2014)
37. L.H. Ahrens, *Geochim. Cosmochim. Acta* **2**, 155 (1952)
38. W. Su, J. Zhang, Z. Feng, T. Chen, P. Ying, C. Li, *J. Phys. Chem. C* **112**, 7710 (2008)
39. S. Challagulla, R. Nagarjuna, R. Ganesan, S. Roy, *ACS Sustain. Chem. Eng.* **4**, 974 (2016)
40. S. Zhang, H. Yang, H. Gao, R. Cao, J. Huang, X. Xu, *ACS Appl. Mater. Interfaces* **9**, 23635 (2017)